Original Research

SIRT2 deficiency prevents age-related bone loss in rats by inhibiting osteoclastogenesis

Yixuan Jing[#], Yanman Zhou[#], Feiye Zhou, Xiaofeng Wang, Bei Tao, Lihao Sun, Jianmin Liu, Hongyan Zhao[*]

Department of Endocrine and Metabolic Diseases, Rui-jin Hospital, Shanghai Jiao-tong University School of Medicine, Shanghai Institute of Endocrine and Metabolic Diseases, Shanghai Clinical Center for Endocrine and Metabolic Diseases, Shanghai, China

Abstract: Sirtuin 2 (SIRT2) is a deacetylase that belongs to class III family of histone deacetylases (HDACs). Although it is the most abundantly expressed member of HDAC-III in human bone tissues, it is unclear whether SIRT2 plays a role in bone metabolism. In this study, the role of SIRT2 in bone metabolism, and the underlying mechanism were investigated. In *in vivo* experiments, micro-CT analysis revealed that there were no differences in bone microstructures between SIRT2-KO and WT rats at 12 weeks of age. However, in 36-week-old rats, increased Tb. BMD, bone volume fraction (BV/TV) and trabecular number (Tb. N) of distal femurs were observed in SIRT2-KO rats, when compared with those of WT rats. Moreover, reduced serum β-CTX was identified in the 36-week old rats. In *in vitro* studies, inhibition of SIRT2 with its specific inhibitor, AGK2, suppressed the differentiation of bone marrow-derived mononuclear cells (BMMs) into osteoclasts via reduction of the expressions of c-Fos and NFATc1. These results suggest that SIRT2 plays a role in age-related bone loss, probably by regulating osteoclastogenesis.

Key words: Sirtuin 2; Bone mineral density; AGK2; Osteoclast.

Introduction

Bone remodeling is regulated by matrix-forming osteoblasts and bone-resorbing osteoclasts under the coordination of various elements such as cytokines, growth factors, adaptor proteins and hormones (1-4). Osteoclasts are giant multi-nucleated cells that differentiate from hematopoietic cell lineages of monocyte/macrophages (5). The formation of mature osteoclasts is governed by macrophage colony-stimulating factor (M-CSF) and receptor activator of nuclear factor-kappa B ligand (RANKL) (6, 7). Under M-CSF induction, RANKL interacts with receptor activator of nuclear factor NF-kB (RANK) expressed on the surface of osteoclast precursors to trigger osteoclastogenesis-associated signals, leading to the upregulation of nuclear factor-κB (NF-κB), pro-osteoclastogenesis factor c-Fos, and master terminal transcription factor T cells c1 (NFATc1) (6, 8-10). Due to abnormal osteoclast recruitment and activation, enhanced bone resorption leads to osteoporosis and other bone-related diseases. The focus of skeletal disease researches have always been to identify new molecules regulating RANK signals, and to explore potential drug targets for inhibition of osteoclast differentiation and function.

Sirtuins (SIRTs) are a family of NAD+-dependent deacetylases that belong to class III of HDACs consisting of seven members (SIRT1–SIRT7). They are involved in regulating numerous biological processes such as lifespan, DNA repair, stress responses, genomic stability, apoptosis and metabolism (11, 12). A previous study has reported that osteoclast-specific deletion of SIRT1 led to increased osteoclast numbers and bone resorption in female mice (13). It has been revealed that among the seven SIRTs, silent information regulator 2 (SIRT2) is the most expressed isoform in adult bone, and also among the least understood (14, 15). The reported biological functions of SIRT2 include adipogenesis, gluconeogenesis, carcinogenesis, as well as its important roles in neuronal degeneration, oxidative stress and inflammatory pathways (14, 16-18). However, the involvement of SIRT2 in the skeleton has never been investigated to date. In the present study, the effect of global SIRT2 knockout (KO) on bone phenotype of Sprague-Dawley (SD) rats, and the underlying mechanism were investigated.

Materials and Methods

Experimental animals

Sprague Dawley (SD) rats were purchased from Biocytogen (Beijing, China). Heterozygous rats of global SIRT2 +/- were produced through clustered, regularly interspaced, short palindromic repeat (CRISPR–CRISPR)-associated protein (Cas) 9-mediated genome modification, which was used to generate SIRT2-KO rats and their wild type (WT) littermates. All rats were maintained in a specific pathogen-free environment and housed in an air-conditioned atmosphere with 12-h day/12-h night cycles, and fed on a normal chow diet. The rats were sacrificed through carbon dioxide inhalation and femur samples were collected for further analysis. The limb bones of 4-week-old female rats were isolated for the extraction of bone marrow stem cells. All

animal protocols were reviewed and approved by the Animal Care Committee of Rui-jin Hospital affiliated to Shanghai Jiao-tong University School of Medicine.

Reagents

Cytochemical staining kits for tartrate-resistant acid phosphatase (TRAP) and AGK2 were purchased from Sigma-Aldrich (St. Louis, USA). Recombinant M-CSF was purchased from Sinobiological (Beijing, China). Soluble recombinant RANKL was obtained from R&D Systems (Minneapolis, USA). Dulbecco's Modified Eagle's medium (DMEM), fetal bovine serum (FBS) and penicillin-streptomycin-glutamine solution were products of Gibco (Grand Island, USA). Antibodies against NFATc1 and SIRT2 were purchased from Santa Cruz Biotechnology (Dallas, Texas, USA), while antibodies against α-tubulin and GAPDH were obtained from Cell Signaling Technology (Danvers, USA). ELISA kits for measuring bone turnover markers were bought from Senxiong BioTech (Shanghai, China).

Micro-comPuted tomograPhy (micro-CT) analysis

The right femurs were isolated from 12-week- and 36-week-old female rats (12-week-old: n = 9 -10 per group; 36-week-old: n = 10 per group). The femurs were fixed in 4% paraformaldehyde (PFA) for one week and stored in 75% ethyl alcohol for micro-CT. The micro-CT analysis was performed using Small Animal Tomographic Analysis facility (SkyScan-1176 μ-CT, Bruker, Kontich, Belgium). The femurs were scanned at a resolution of 7.93 μm per voxel, 180° scan, 1 mm optical filter, 70 kV, 278 μA and 450 ms exposure. The regions of interest (ROI) were quantitatively analyzed from 0.5 mm to 2.7 mm above the medial and lateral growth plates at the distal metaphysis. The NRecon Software was used to reconstruct and visualize the image data, while the parameters were quantified using CTan Evaluation Software.

Hematoxylin and eosin (HE) staining

The left femurs were isolated from 36-week-old female rats, fixed in 4% PFA for 48 hours, and decalcified by transfer into 15% ethylene diamine tetraacetic acid (EDTA). The decalcified femurs were embedded in paraffin (when it was ascertained that a fine needle could be smoothly inserted into the bone tissues). After coagulation, the embedded blocks were sliced along the longitudinal axis of the bone at a thickness of 6 μm, and subjected to H&E staining.

Serum levels of bone turnover markers

Whole blood was extracted from the heart of 36-week-old rats, and serum was obtained through centrifugation after keeping it standing at room temperature for 2 hours. The concentrations of serum bone formation marker procollagen type 1 N-terminal pro-peptide (P1NP) and bone resorption marker C-terminal cross-linking telopeptide of type I collagen (β-CTX) were measured using their respective ELISA kits.

Cell culture and osteoclast differentiation

Whole bone marrow cells were isolated from limb-long bones of 4-week-old female rats, including humeri, femurs and tibias. Bone marrow cells were plated in DMEM supplemented with 10% FBS and 1 x 1% penicillin-streptomycin-glutamine solution in a 5% CO_2 atmosphere at 37°C overnight. Then, the culture medium was replaced with fresh medium containing recombinant 30 ng/ml M-CSF. After culturing for 5 days, a mass of BMMs were proliferated.

For osteoclast differentiation, BMMs were seeded into 24-well plates at a density of 1×10^5 cells/well, and stimulated with DMEM containing 50 ng/ml RANKL and 30 ng/ml M-CSF. The culture medium was changed every 2 days for a total of 6 days, and TRAP staining was performed to identify osteoclasts according to protocols of the manufacturer. Multinucleated cells with three or more nuclei were defined as TRAP-positive cells, and the number of nuclei were counted in randomly selected fields. The Fusion Index of osteoclasts was calculated as follows:

$$Fusion\ Index\ (\%) = \frac{Number\ of\ nuclei\ (TRAP-positive\ cells) \times 100}{Number\ of\ nuclei\ (field\ of\ vision)}$$

Cell viability assay

The BMMs were seeded into 96-well plates at a density of 2.5×10^4 cells/well, and treated with graded concentrations of AGK2 (1, 2.5, 5.0, 7.5, 10.0, 12.5 and 15 μM) in the presence of M-CSF (30 ng/ml) for 12, 24 or 48 hours. Untreated BMMs served as control. Cell viability assay was performed using Cell Counting Kit-8 (Dojindo, Japan) in line with the manufacturer's instructons. Absorbance was measured at 450 nm using an automatic microplate reader (CLARIOstar, BMG Lab-Tech, Germany).

Treatment with inhibitors

The BMMs were cultured in the presence of 30 ng/ml M-CSF for 48 hours. Then, the negative control group (30 ng/ml M-CSF group), positive control group (30 ng/ml M-CSF group given 50 ng/ml RANKL) and treatment group (30 ng/ml M-CSF group given 50 ng/ml RANKL and 10 μmol/L AGK2) were set up, with their respective treatments in DMEM. The medium was changed every 2 days for a total of 6 days.

Quantitative real-time PCR (qPCR)

The BMMs were seeded into 12-well plates at a density of 2×10^5 cells/well, and cultured as described earlier. Total RNA was extracted using TRI-Reagent (Sigma-Aldrich, USA). The RNA was reverse-transcribed into cDNA following the instructions of PrimeScript™ RT Master Mix (Takara, Japan). The mRNA levels of osteoclast markers were quantified using qPCR with SYBR Premix Ex Taq™ (Takara, Japan) in a LightCycler® 480 Real-Time PCR System (Rocha, USA). The sequences of the primers used were: β-actin: forward: 5'-CCACCATGTACC-CAGGCATT -3', reverse: 5'-CGGACTCATCG-TACTCCTGC-3'; SIRT2: forward: 5'-GAATTC-GAGATGGACTTCCTACGG-3', reverse: 5'-CTC-GAGCTAGTGTTCCTCTTTCTCTTTG-3'; TRAP: forward: 5'-ACGGCTACTTGCGGTTCAC-3', reverse 5':TCCTTGGGAGGCTGGTCTTA-3'; ITGαVβ3: forward: 5'-CAAGATTGGAGACACGTGA-3', r verse: 5'CCTGGACTGTAAGG TGTCC-3'; NFATc1: forward 5'-AGCCATCATCGACTGTGCTG-3', reverse: 5'-GGATGTGGACTCGGAAGACC-3'; c-Fos:

forward 5'-ACGTGGAGCTGAAGGCAGAAC-3', reverse: 5'-AGCCACTGGGCCTAGATGATG-3'; RANK: forward 5'-GGCTGGCTACCACTGGA CT-3', reverse: 5'-TCCTGTAGTAAACGCCGAAGA-3'; CAII: forward 5'-CCAGTTTCACTTTCACTG-3', reverse: 5'-AGGCAGGTCCAATCTTCAA-3', and Cathepsin K: forward 5'-TAATGTGAACCATG CGTGT-3', reverse: 5'-CGAGCCAAGAGAACA-TAGCC-3'.

Western blotting

The BMMs were seeded into 6-well plates at a density of 4×10^5 cells/well, and cultured as described earlier. The cells were lysed in cold radioimmunoprecipitation assay (RIPA) buffer (Beyotime Biotechnology, China) containing phenylmethylsulfonyl fluoride (PMSF) (Beyotime Biotechnology, China) for 30 min. The cell lysate was centrifuged at 12,000 rpm for 15 min at 4°C, and the protein concentration was determined using the bicinchoninic acid (BCA) assay kit (Pierce BCA Protein Assay Kit, Thermo Scientific, USA). Samples were separated by subjecting them to sodium dodecyl sulfate-polyacrylamide gel electrophoresis (SDS-PAGE), and transferred to polyvinylidene difluoride (PVDF) membranes (Thermo Scientific, USA). The membranes were blocked with 5% non-fat milk in Tris buffered saline-Tween 20 (TBST). , and then incubated with primary antibodies at 4 °C overnight, after which the membranes were washed and incubated with secondary antibodies for 1 h.The blots were visualized using an enhanced chemiluminescence (ECL) detection system (Tanon Science & Technology, China).

Statistical analysis

Data are expressed as mean ± standard deviation (SD). One-way ANOVA or two-tailed Student's *t*-test was performed to compare groups. Statistical significance was established at $p < 0.05$.

Results

Effect of SIRT2-KO on bone phenotype

Global SIRT2-KO and WT rats were identified through genotyping (Figure 1A). The SIRT2-KO had no impact on body weight and bone length in 12-week-old and 36-week-old SIRT2-KO female rats (Figure 1B-1D). Micro-CT analysis revealed no difference in bone microstructures between 12-week-old SIRT2-KO and WT rats. However, when 36-week-old SIRT2-KO rats were compared with age-macthed WT rats, statistical differences were observed in Tb. BMD (WT: 0.17 ± 0.04 g/cm³, KO: 0.19 ± 0.02 g/cm³, $p < 0.05$) and trabecular bone volume fraction (BV/TV%) (WT: 8.3 ± 5.4, KO: 12.0 ± 8.6, $p < 0.05$). These results are shown in Figure 2A and Figure 2B. The higher BV/TV resulted from an increased trabecular number (Tb. N) (WT: 1.0 ± 0.4 mm⁻¹, KO: 1.5 ± 0.6 mm⁻¹, $p < 0.05$), with no significant change in trabecular thickness (Tb. Th) and trabecular spacing (Tb. Sp) (Figure 2D-2F). Bone surface area/tissue volume (BS/TV) displayed an increasing trend, while trabecular bone pattern factor (Tb. Pf) and structure model index (SMI) showed decreasing trends in SIRT2-KO rats, although the differences were not statistically significant (Figure 2C, Figure 2G and Fi-
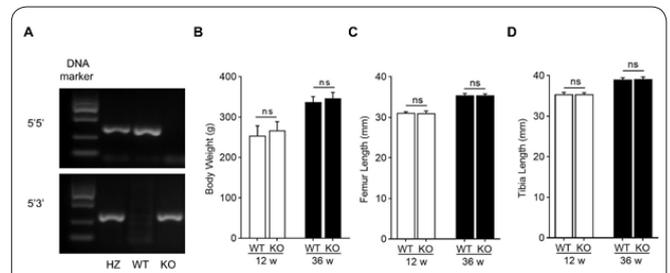

Figure 1. Genotype identification, body weight and bone length in SIRT2 KO female rats and age-matched WT rats. A: Genomic DNA determined using qPCR. (B) Body weight (g); C and D: femur and tibia length (mm). Data are expressed as mean ± SD (n = 9-10 per group). (ns: no significance versus WT group; HZ: heterozygote; WT: wild type; KO: SIRT2 knockout).
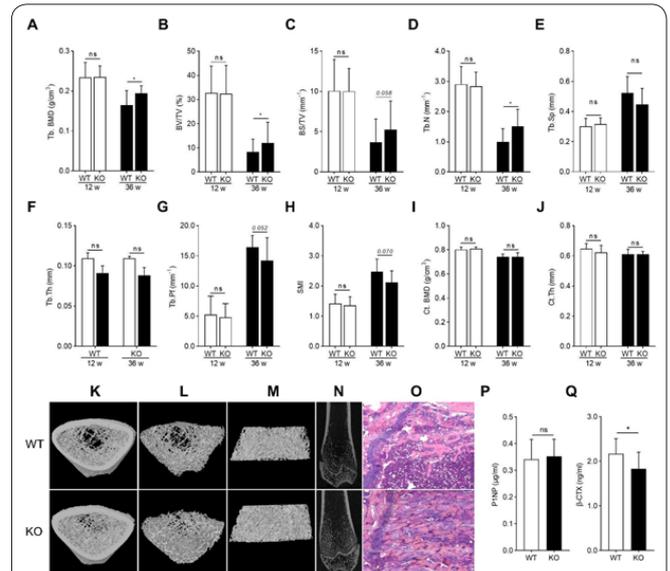

Figure 2. Bone microstructures of femurs of SIRT2 KO female rats and age-matched WT rats. A: Tb. BMD (g/cm³), trabecular bone mineral density; B: BV/TV (%), bone volume per total volume; C: BS/TV (mm⁻¹), bone surface per total volume; D: Tb. N (mm⁻¹), trabecular number; E: Tb. Sp (mm), trabecular spacing; F: Tb. Th (mm), trabecular thickness; G: Tb. Pf (mm⁻¹), trabecular bone pattern factor; H: SMI, structure model index; I: Ct. BMD (g/cm³), cortical bone mineral density; J: Ct. Th (mm), cortical thickness; K-N: Representative reconstruction micro-CT images of distal femurs metaphysis of rats aged 36 weeks. K: Cross-sectional images of cortical with cancellous bone area; L: Cross-sectional images of trabecular bone area; M: Longitudinal images of trabecular bone area; N: Longitudinal two-dimensional structures of femurs distal metaphysis. O: HE staining for bone tissues near epiphyseal plates of rats aged 36 weeks (the arrows show the growth plates); P: P1NP, serum bone formation marker procollagen type 1 N-terminal pro-peptide of female rats aged 36 weeks; Q: β-CTX, serum bone resorption marker C-terminal cross-linking telopeptide of type I collagen of female rats aged 36 weeks. Data are expressed as mean ± SD (n = 9-10 per group). *$p < 0.05$, versus WT group. (ns: no significance versus WT group; WT: wild type; KO: SIRT2 knockout).

gure 2H). Moreover, micro-CT analysis showed limited differences in cortical BMD (Ct. BMD) and thickness (Ct. Th) between SIRT2-KO and WT rats (Figure 2I and Figure 2J). The comparison can be seen in representative micro-CT images of the distal femurs (Figures 2K -2N). Moreover, HE staining near the epiphyseal plates showed similar results in 36-week-old female rats (Figure 2O).

Reduced serum levels of β-CTX in SIRT2-KO rats aged 36 weeks

Decreased levels of bone resorption marker β-CTX were identified in SIRT2-KO rats aged 36 weeks, when compared with that of WT rats (WT: 2.2 ± 0.3 μg/ml, KO: 1.8 ± 0.4 μg/ml, $p < 0.05$), indicating less activated bone resorption in SIRT2-KO rats (Figure 2Q). No difference was found regarding P1NP, the bone formation marker (Figure 2P).

AGK2 had no impact on BMM viability

As a specific inhibitor of SIRT2, AGK2 produced no cytotoxicity in BMMs at concentrations up to 15 μM in the presence of M-CSF (Figures 3A-3C). The concentration of AGK2 used in previous studies (10 μM) was chosen in subsequent experiments (19, 20).

AGK2 inhibited the expression of SIRT2 at protein level

In order to investigate the inhibitory effect of AGK2 on SIRT2, BMMs were cultured with 10 μM AGK2. Results from qPCR and western blotting revealed that RANKL induced the mRNA expression of SIRT2 (Figure 4A); treatment with AGK2 suppressed SIRT2 protein expression level rather than mRNA expression level (Figures 4A and 4B).

Suppression of SIRT2 inhibited RANKL stimulated osteoclastogenesis in vitro

Results from TRAP staining showed that teatment with 10 μM AGK2 (MR+AGK2) significantly reduced osteoclast differentiation and the formation of TRAP-positive multinuclear osteoclasts, when compared with the positive control (MR) (Figure 5A and Figure 5B). In addition, AGK2 supressed the mRNA expressions of osteoclast differentiation-associated biomarkers TRAP and ITGαvβ3 (Figures 5C, 5D and 5G).

AGK2 inhibited c-Fos and NFATc1 expression during RANKL stimulated osteoclastogenesis in vitro

The molecular mechanism by which AGK2 suppressed RANKL-induced osteoclastogenesis was also investigated. Studies have shown that NFATc1, a downstream regulatory factor of c-Fos, is a master transcription factor that manages the terminal period of RANKL-mediated osteoclastogenesis (8, 21). The mRNA expressions of c-Fos and NFATc1 were downregulated by teatment with 10 μM AGK2 (Figures 5H and 5I). Consistent with these results, the protein ex-
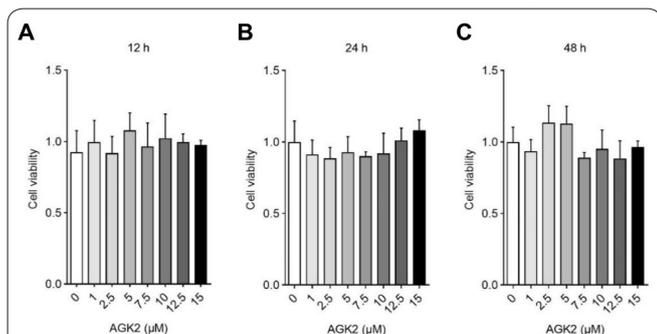
pression of NFATc1 decreased as well (Figure 5J).

Discussion

To the best of our knowledge, this is the first study providing evidence for the significant role of SIRT2 in regulating bone metabolism and bone-related cells. Quantitative analyses of micro-CT revealed that SIRT2 deficiency led to bone microstructural effects in rats aged 36 weeks rather than those aged 12 weeks. Rats reach peak bone mass at 12-14 weeks of age, after which the bone mass starts to decrease (22, 23). This is consistent with the results obtained in the present study which showed that 36-week rats had lower bone mass
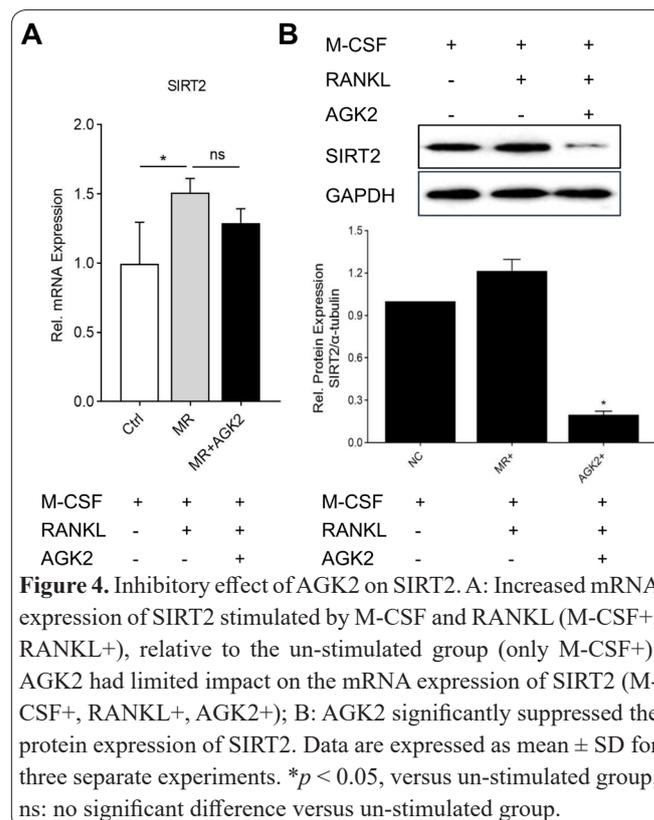
Figure 4. Inhibitory effect of AGK2 on SIRT2. A: Increased mRNA expression of SIRT2 stimulated by M-CSF and RANKL (M-CSF+, RANKL+), relative to the un-stimulated group (only M-CSF+). AGK2 had limited impact on the mRNA expression of SIRT2 (M-CSF+, RANKL+, AGK2+); B: AGK2 significantly suppressed the protein expression of SIRT2. Data are expressed as mean ± SD for three separate experiments. *$p < 0.05$, versus un-stimulated group; ns: no significant difference versus un-stimulated group.
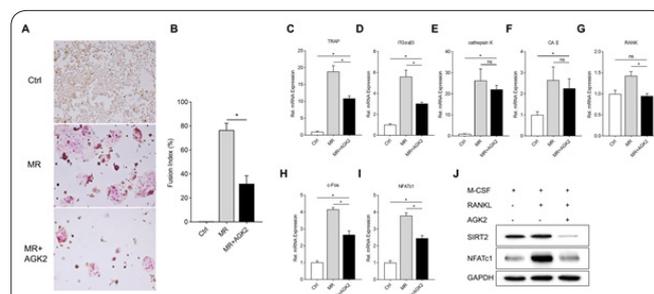
Figure 5. Suppression of SIRT2 inhibited RANKL-induced osteoclastogenesis. A: Reduced formation of TRAP-positive multinuclear osteoclasts by 10 μM AGK2. Ctrl: negative control group (M-CSF only); MR: positive control group (M-CSF and RANKL); MR+AGK2, treatment group (M-CSF, RANKL and AGK2). B: Osteoclasts Fusion Index. C-F: AGK2 suppressed RANKL-induced expressions of specific osteoclast differentiation markers. G-I: AGK2 suppressed RANKL-induced mRNA expression of the specific receptor, RANK, crucial transcription factors c-Fos and NFATc1. (J) J: AGK2 suppresses the RANKL-induced protein expression of NFATc1. Data are expressed as mean ± SD. * $p < 0.05$ versus Ctrl or MR groups. (ns = no significant difference versus Ctrl or MR groups).

Figure 3. Effect of AGK2 on cell viability. A-C: BMMs cultured with various concentrations of AGK2 (up to 15 μM) for 12, 24 or 48 hours in the presence of M-CSF. AGK2 had no impact on cell viability, as determined using Cell Counting Kit-8.

and poorer bone microstructure than 12-week-old rats. These results suggest that SIRT2 deficency has no impact on peak bone mass, but may provide a protective effect against furture bone loss. In 36-week-old rats, increased BV/TV directly reflected maintenance of bone mass, whereas the smaller Tb.Pf and SMI values represented plate-like rather than rod-like bone structures, with the structural stability of the former being better than that of the latter (24). After 12 weeks of age, the bone mass of rats gradually decreased due to excessive bone resorption and/or reduced bone formation. Interestingly, it was found that PINP, the bone formation index, did not change, but β-CTX, the bone resorption index, was reduced in SIRT2 knockout rats aged 36 weeks. So, it can be speculated that SIRT2 may be involved in bone metabolism through the regulation of bone resorption. In order to verify the *in vivo* results and investgate the underlying mechanisms, *in vitro* experiments were carried out on the effect of SIRT2 selective inhibitor AGK2 on osteoclast differentiation. The results showed that without affecting the viability of osteoclast precursor cells *in vitro*, RANKL-induced osteoclastogenesis was significantly impaired by AGK2 treatment. Downregulations of RANK and NFATc1 are central features of SIRT2 inhibition. These findings suggest that SIRT2 regulates skeletal homeostasis by regulating osteoclastogenesis.

In recent years, members of HDACs have been investigated as molecular targets for various disorders (15, 25, 26). Among the seven SIRTs of class III HDACs, SIRT1 and SIRT6 have been reported to be associated with skeletal health. It has been reported that activation of SIRT1 promoted the differentistion of mesenchymal stem cells into osteoblasts, while its deletion reduced bone formation and increased bone resorption (13, 27). Mice deficient in SIRT6 had 30% lower bone mineral density (BMD), crooked spine and reduced growth plate chondrocyte proliferation (28). Interestingly, even though it is the most prominently expressed SIRTs in both human skeleton and articular cartilage, the role of SIRT2 in bone metabolism has barely been investigeted (15). The present study provides novel evidence for the regulatory effect of SIRT2 on osteoclastogenesis, revealing that suppression of SIRT2 led to reduced production of RANK, c-Fos and NFATc1. During osteoclastogenesis, all osteoclast target molecules are stimulated by the activation of RANK (29, 30). Evoked by RANK signals, c-Fos promotes NFATc1 expression by binding to the promoter region of the NFATc1 gene. The activated NFATc1 then masters the terminal differentiation of osteoclasts, promoting cell fusion and bone resorption (21, 31-34). Thus, SIRT2 inhibition may be involved in the latter period of RANKL-stimulated osteoclastogenesis. In addition, as a small molecular SIRT modulator, AGK2 is currently considered an effective agent in managing neurodegeneration, malignant tumors, myocardial infarction, obesity and age-related disorders (35). The present has study identified a potential role of AGK2 in managing skeletal disorders via the inhibition of SIRT2. It can ve reasonably speculated, based on the *in vitro* and *in vivo* results, that with decrease in bone mass after reaching peak bone mass, deficiency/reduction of/in SIRT2 serves a protective role due to reduced activition of osteoclasts-mediated bone resorption.

The enhanced phenotypic features of global SIRT2-KO rats support a physiological role of SIRT2 in age-related bone loss. The reduction of serum β-CTX, along with the inhibitory effect of SIRT2 suppression on osteoclastogenesis, suggest that SIRT2 may function in the management of skeletal homeostasis through its effect on osteoclasts. Thus, suppression of SIRT2 may provide a promising therapeutic strategy for age-related bone loss. Further studies are needed to investigate whether SIRT2-specific deletion in osteoclasts would still influence skeletal phenotype and cell differentiation, as well as the potential of AGK2 as a therapeutic agent for skeletal disorders.

Acknowledgements

Conflict of Interest
There are no conflict of interest in this study.

Author's contribution
All work was done by the author s named in this article and the authors accept all liability resulting from claims which relate to this article and its contents. The study was conceived and designed by Hongyan Zhao; Yixuan Jing, Yanman Zhou, Feiye Zhou, Xiaofeng Wang, Bei Tao, Lihao Sun, Hongyan Zhao collected and analysed the data; Yixuan Jing and Yanman Zhou wrote the text and all authors have read and approved the text prior to publication.
Yixuan Jing and Yanman Zhou contributed equally to this work and should be considered as co-first authors.

References

1. Zaidi M. Skeletal remodeling in health and disease. Nat Med 2007; 7: 791-801.

2. Berendsen AD, Olsen BR. Bone development. Bone 2015: 14-18.

3. Rastogi A, Hajela A, Prakash M, Khandelwal N, Kumar R, Bhattacharya A, et al. Teriparatide (recombinant human parathyroid hormone [1-34]) increases foot bone remodeling in diabetic chronic Charcot neuroarthropathy: a randomized double-blind placebo-controlled study. Journal of diabetes 2019.

4. Portillo-Sanchez P, Bril F, Lomonaco R, Barb D, Orsak B, Bruder JM, et al. Effect of pioglitazone on bone mineral density in patients with nonalcoholic steatohepatitis: A 36-month clinical trial. Journal of diabetes 2019; 3: 223-231.

5. Teitelbaum SL. Bone resorption by osteoclasts. Science 2000; 5484: 1504-8.

6. Yang X, Pande S, Scott C, Friesel R. Macrophage colony-stimulating factor pretreatment of bone marrow progenitor cells regulates osteoclast differentiation based upon the stage of myeloid development. J Cell Biochem 2019.

7. Lacey DL, Timms E, Tan HL, Kelley MJ, Dunstan CR, Burgess T, et al. Osteoprotegerin ligand is a cytokine that regulates osteoclast differentiation and activation. Cell 1998; 2: 165-76.

8. Boyce BF, Yamashita T, Yao Z, Zhang Q, Li F, Xing L. Roles for NF-kappaB and c-Fos in osteoclasts. J Bone Miner Metab 2005: 11-5.

9. Park JH, Lee NK, Lee SY. Current Understanding of RANK Signaling in Osteoclast Differentiation and Maturation. Mol Cells 2017; 10: 706-713.

10. Kim JH, Kim N. Regulation of NFATc1 in Osteoclast Differentiation. J Bone Metab 2014; 4: 233-41.

11. Michan S, Sinclair D. Sirtuins in mammals: insights into their biological function. Biochem J 2007; 1: 1-13.

12. Finkel T, Deng CX, Mostoslavsky R. Recent progress in the biology and physiology of sirtuins. Nature 2009; 7255: 587-91.

13. Edwards JR, Perrien DS, Fleming N, Nyman JS, Ono K, Connelly L, et al. Silent information regulator (Sir)T1 inhibits NF-kappaB signaling to maintain normal skeletal remodeling. Journal of bone and mineral research : the official journal of the American Society for Bone and Mineral Research 2013; 4: 960-9.

14. Gomes P, Fleming Outeiro T, Cavadas C. Emerging Role of Sirtuin 2 in the Regulation of Mammalian Metabolism. Trends Pharmacol Sci 2015; 11: 756-768.

15. Bradley EW, Carpio LR, van Wijnen AJ, McGee-Lawrence ME, Westendorf JJ. Histone Deacetylases in Bone Development and Skeletal Disorders. Physiol Rev 2015; 4: 1359-81.

16. Outeiro TF, Kontopoulos E, Altmann SM, Kufareva I, Strathearn KE, Amore AM, et al. Sirtuin 2 inhibitors rescue alpha-synuclein-mediated toxicity in models of Parkinson's disease. Science 2007; 5837: 516-9.

17. Park SH, Zhu Y, Ozden O, Kim HS, Jiang H, Deng CX, et al. SIRT2 is a tumor suppressor that connects aging, acetylome, cell cycle signaling, and carcinogenesis. Transl Cancer Res 2012; 1: 15-21.

18. Zhou Z, Ma T, Zhu Q, Xu Y, Zha X. Recent advances in inhibitors of sirtuin1/2: an update and perspective. Future Med Chem 2018; 8: 907-934.

19. Li Y, Nie H, Wu D, Zhang J, Wei X, Ying W. Poly(ADP-ribose) polymerase mediates both cell death and ATP decreases in SIRT2 inhibitor AGK2-treated microglial BV2 cells. Neurosci Lett 2013: 36-40.

20. Thangjam GS, Birmpas C, Barabutis N, Gregory BW, Clemens MA, Newton JR, et al. Hsp90 inhibition suppresses NF-kappaB transcriptional activation via Sirt-2 in human lung microvascular endothelial cells. Am J Physiol Lung Cell Mol Physiol 2016; 10: L964-74.

21. Takayanagi H, Kim S, Koga T, Nishina H, Isshiki M, Yoshida H, et al. Induction and activation of the transcription factor NFATc1 (NFAT2) integrate RANKL signaling in terminal differentiation of osteoclasts. Dev Cell 2002; 6: 889-901.

22. Zhu BY, Yang ZD, Chen XR, Zhou J, Gao YH, Xian CJ, et al. Exposure Duration Is a Determinant of the Effect of Sinusoidal Electromagnetic Fields on Peak Bone Mass of Young Rats. Calcif Tissue Int 2018; 1: 95-106.

23. Fournier C, Rizzoli R, Ammann P. Low calcium-phosphate intakes modulate the low-protein diet-related effect on peak bone mass acquisition: a hormonal and bone strength determinants study in female growing rats. Endocrinology 2014; 11: 4305-15.

24. Moon HS, Won YY, Kim KD, Ruprecht A, Kim HJ, Kook HK, et al. The three-dimensional microstructure of the trabecular bone in the mandible. Surg Radiol Anat 2004; 6: 466-73.

25. Falkenberg KJ, Johnstone RW. Histone deacetylases and their inhibitors in cancer, neurological diseases and immune disorders. Nat Rev Drug Discov 2014; 9: 673-91.

26. McGee-Lawrence ME, Westendorf JJ. Histone deacetylases in skeletal development and bone mass maintenance. Gene 2011; 1-2: 1-11.

27. Backesjo CM, Li Y, Lindgren U, Haldosen LA. Activation of Sirt1 decreases adipocyte formation during osteoblast differentiation of mesenchymal stem cells. Cells Tissues Organs 2009; 1-4: 93-7.

28. Piao J, Tsuji K, Ochi H, Iwata M, Koga D, Okawa A, et al. Sirt6 regulates postnatal growth plate differentiation and proliferation via Ihh signaling. Sci Rep 2013: 3022.

29. Hsu H, Lacey DL, Dunstan CR, Solovyev I, Colombero A, Timms E, et al. Tumor necrosis factor receptor family member RANK mediates osteoclast differentiation and activation induced by osteoprotegerin ligand. Proc Natl Acad Sci U S A 1999; 7: 3540-5.

30. Boyle WJ, Simonet WS, Lacey DL. Osteoclast differentiation and activation. Nature 2003; 6937: 337-42.

31. Kim K, Kim JH, Lee J, Jin HM, Lee SH, Fisher DE, et al. Nuclear factor of activated T cells c1 induces osteoclast-associated receptor gene expression during tumor necrosis factor-related activation-induced cytokine-mediated osteoclastogenesis. J Biol Chem 2005; 42: 35209-16.

32. Wang ZQ, Ovitt C, Grigoriadis AE, Mohle-Steinlein U, Ruther U, Wagner EF. Bone and haematopoietic defects in mice lacking c-fos. Nature 1992; 6406: 741-5.

33. Asagiri M, Takayanagi H. The molecular understanding of osteoclast differentiation. Bone 2007; 2: 251-64.

34. Kim K, Lee SH, Ha Kim J, Choi Y, Kim N. NFATc1 induces osteoclast fusion via up-regulation of Atp6v0d2 and the dendritic cell-specific transmembrane protein (DC-STAMP). Mol Endocrinol 2008; 1: 176-85.

35. Bai X, Yao L, Ma X, Xu X. Small Molecules as SIRT Modulators. Mini Rev Med Chem 2018; 13: 1151-1157.